A Correlation for Interfacial Heat Transfer Coefficient for Turbulent Flow Over an Array of Square Rods

Marcelo B. Saito

Marcelo J. S. de Lemos[1]
Mem. ASME
e-mail: delemos@ita.br

Departamento de Energia - IEME,
Instituto Tecnológico de Aeronáutica - ITA,
12228-900 - São José dos Campos - SP, Brazil

Interfacial heat transfer coefficients in a porous medium modeled as a staggered array of square rods are numerically determined. High and low Reynolds k-ϵ turbulence models are used in conjunction of a two-energy equation model, which includes distinct transport equations for the fluid and the solid phases. The literature has documented proposals for macroscopic energy equation modeling for porous media considering the local thermal equilibrium hypothesis and laminar flow. In addition, two-energy equation models have been proposed for conduction and laminar convection in packed beds. With the aim of contributing to new developments, this work treats turbulent heat transport modeling in porous media under the local thermal nonequilibrium assumption. Macroscopic time-average equations for continuity, momentum, and energy are presented based on the recently established double decomposition concept (spatial deviations and temporal fluctuations of flow properties). The numerical technique employed for discretizing the governing equations is the control volume method. Turbulent flow results for the macroscopic heat transfer coefficient, between the fluid and solid phase in a periodic cell, are presented. [DOI: 10.1115/1.2175150]

Keywords: turbulence modeling, porous media, heat transfer coefficient

1 Introduction

Convection heat transfer in porous media has been extensively investigated due to its many important engineering applications. The wide applications available have led to numerous investigations in this area. Such applications can be found in solar receiver devices, building thermal insulation, heat exchangers, energy storage units, etc. From the point of view of the energy equation there are two different models, local thermal equilibrium model and the two energy approach. The first model assumes that the solid temperature is equal to the fluid temperature, thus local thermal equilibrium between the fluid and the solid-phases is achieved at any location in the porous media. This model simplifies theoretical and numerical research, but the assumption of local thermal equilibrium between the fluid and the solid is inadequate for a number of problems [1–4]. In recent years more attention has been paid to the local thermal nonequilibrium model and its use has increased in theoretical and numerical research for convection heat transfer processes in porous media [5,6].

Kuwahara et al. [7] proposed a numerical procedure to determine macroscopic transport coefficients from a theoretical basis without any empiricism. They used a single unit cell and determined the interfacial heat transfer coefficient for the asymptotic case of infinite conductivity of the solid phase. Nakayama et al. [8] extended the conduction model of Hsu [9] for treating also convection in porous media and the monographs of [3,10,11] fully document forced convection in porous media. Having established the macroscopic energy equations for both phases, useful exact solutions were obtained for two fundamental heat transfer processes associated with porous media, namely, steady conduction in a porous slab with internal heat generation within the solid, and also, thermally developing flow through a semi-infinite porous medium. Sahraouri and Kaviany [12] performed direct numerical simulations of premixed combustion in a two-dimensional porous medium made of in-line and staggered arrangements of square cylinders. Results therein were limited to the laminar flow regime.

Saito and de Lemos [13] considered local thermal nonequilibrium and obtained the interfacial heat transfer coefficient for laminar flow using a single unit cell with local instantaneous transport equations.

In all of the above, only laminar flow has been considered. When treating turbulent flow in porous media, however, difficulties arise due to the fact that the flow fluctuates with time and a volumetric average is applied [14]. For handling such situations, a new concept called *double decomposition* has been proposed for developing macroscopic models for turbulent transport in porous media [15–19]. This methodology has been extended to nonbuoyant heat transfer [20], buoyant flows [21–24], mass transfer [25], and double diffusion [26]. In addition, a general classification of models has been published [27]. Recently, the problem of treating interfaces between a porous medium and a clear region, considering a diffusion-jump condition for laminar [28] and turbulence fields [29–31], have also been investigated under the concept first proposed by [15–19]. Following this same concept, de Lemos and Rocamora [32] have developed a macroscopic turbulent energy equation for a homogeneous, rigid, and saturated porous medium, considering local thermal equilibrium between the fluid and solid matrix.

Motivated by the foregoing, this work focuses on turbulent flow through a packed bed, which represents an important configuration for efficient heat and mass transfer and suggests the use of equations governing thermal nonequilibrium involving distinct energy balances for both the solid and fluid phases. Accordingly, the use of such two-energy equation model requires an extra parameter to be determined, namely, the heat transfer coefficient between the fluid and the solid. The contribution herein consists in proposing a new correlation for obtaining the interfacial heat transfer coefficient for turbulent flow in a packed bed. The bed is

[1]Corresponding author.

Contributed by the Heat Transfer Division of ASME for publication in the JOURNAL OF HEAT TRANSFER. Manuscript received April 15, 2005; final manuscript received October 28, 2005. Review conducted by N.K. Anand.

modeled as an infinite staggered array of square rods and the range of Reynolds number, based on the size of the rod, is extended up to 10^7. In-line rod arrangement is not considered here as the objective of this work to first consolidate results for staggered arrays. Future investigations shall consider different array arrangements as well as distinct rod shapes, such as elliptical and circular rods.

The next sections detail the basic mathematical model, including the mean and turbulent fields for turbulent flows. Although the discussion of turbulent motion in porous media is not presented in this work, the definitions and concepts to calculate the interfacial heat transfer coefficient for macroscopic flows are presented.

2 Governing Equations

2.1 Microscopic Transport Equations. Microscopic transport equations or local time-averaged transport equations for incompressible fluid flow in a rigid homogeneous porous medium have already been presented in the literature and for that they are just presented here [32]. The governing equations for the flow and energy for an incompressible fluid are given by:

Continuity:

$$\nabla \cdot \mathbf{u} = 0 \tag{1}$$

Momentum:

$$\rho\left[\frac{\partial \mathbf{u}}{\partial t} + \nabla \cdot (\mathbf{uu})\right] = -\nabla p + \mu \nabla^2 \mathbf{u} \tag{2}$$

Energy-fluid phase:

$$(\rho c_p)_f \left\{\frac{\partial T_f}{\partial t} + \nabla \cdot (\mathbf{u} T_f)\right\} = \nabla \cdot (k_f \nabla T_f) + S_f \tag{3}$$

Energy-solid phase (porous matrix):

$$(\rho c_p)_s \frac{\partial T_s}{\partial t} = \nabla \cdot (k_s \nabla T_s) + S_s \tag{4}$$

where the subscripts f and s refer to fluid and solid phases, respectively. Here, T is the temperature, k_f is the fluid thermal conductivity, k_s is the solid thermal conductivity, c_p is the specific heat, and S is the heat generation term. If there is no heat generation either in the solid or in the fluid, one has further $S_f = S_s = 0$.

For turbulent flows the time averaged transport equations can be written as:

Continuity:

$$\nabla \cdot \bar{\mathbf{u}} = 0 \tag{5}$$

Momentum:

$$\rho_f[\nabla \cdot (\overline{\mathbf{uu}})] = -\nabla \bar{p} + \nabla \cdot \{\mu[\nabla \bar{\mathbf{u}} + (\nabla \bar{\mathbf{u}})^T] - \rho \overline{\mathbf{u}'\mathbf{u}'}\} \tag{6}$$

where the low and high Reynolds k-ϵ model is used to obtain the eddy viscosity, μ_t, whose equations for the turbulent kinetic energy per unit mass and for its dissipation rate read:

Turbulent kinetic energy per unit mass:

$$\rho_f[\nabla \cdot (\bar{\mathbf{u}} k)] = \nabla \cdot \left[\left(\mu + \frac{\mu_t}{\sigma_k}\right) \nabla k\right] - \rho \overline{\mathbf{u}'\mathbf{u}'} : \nabla \bar{\mathbf{u}} - \rho \epsilon \tag{7}$$

Turbulent kinetic energy per unit mass dissipation rate:

$$\rho_f[\nabla \cdot (\bar{\mathbf{u}} \epsilon)] = \nabla \cdot \left[\left(\mu + \frac{\mu_t}{\sigma_\epsilon}\right) \nabla \epsilon\right] + [c_1(-\rho \overline{\mathbf{u}'\mathbf{u}'} : \nabla \bar{\mathbf{u}}) - c_2 f_2 \rho \epsilon] \frac{\epsilon}{k} \tag{8}$$

Reynolds stresses and the eddy viscosity is given by, respectively,

$$-\rho \overline{\mathbf{u}'\mathbf{u}'} = \mu_t[\nabla \bar{\mathbf{u}} + (\nabla \bar{\mathbf{u}})^T] - \frac{2}{3}\rho k \mathbf{I} \tag{9}$$

$$\mu_t = \rho c_\mu f_\mu \frac{k^2}{\epsilon} \tag{10}$$

where, ρ is the fluid density, p is the pressure, μ represents the fluid viscosity.

In the above equation set σ_k, σ_ϵ, c_1, c_2, and c_μ are dimensionless constants, whereas f_2 and f_μ are damping functions. The turbulence model constants are

$$c_\mu = 0.09, \quad c_1 = 1.5, \quad c_2 = 1.9, \quad \sigma_k = 1.4, \quad \sigma_\epsilon = 1.3$$

For the high Re model the standard constants of Launder and Spalding [33] were employed.

Also, the time averaged energy equations become:

Energy-fluid phase:

$$(\rho c_p)_f[\nabla \cdot (\bar{\mathbf{u}} \bar{T}_f)] = \nabla \cdot (k_f \nabla \bar{T}_f) - (\rho c_p)_f \nabla \cdot (\overline{\mathbf{u}' T_f'}) \tag{11}$$

Energy-solid phase (porous matrix):

$$\nabla \cdot (k_s \nabla \bar{T}_s) + S_s = 0 \tag{12}$$

2.2 Decomposition of Flow Variables in Space and Time. Macroscopic transport modeling of incompressible flows in porous media has been based on the volume-average methodology for either heat [34] or mass transfer [35,36]. If time fluctuations of the flow properties are also considered, in addition to spatial deviations, there are two possible methodologies to follow in order to obtain macroscopic equations: (a) application of time-average operator followed by volume-averaging [37–42], or (b) use of volume-averaging before time-averaging is applied [43–45]. However, both sets of macroscopic mass transport equations are equivalent when examined under the recently established double decomposition concept [15–19]. As mentioned, the double decomposition concept has been published in a number of worldwide available journal articles [15–32] and does not need to be repeated here.

2.3 Macroscopic Flow and Energy Equations. When the average operators are simultaneously applied over Eqs. (1) and (2), macroscopic equations for turbulent flow are obtained. Volume integration is performed over a REV Refs. [14,46], resulting in

Continuity:

$$\nabla \cdot \bar{\mathbf{u}}_D = 0 \tag{13}$$

where, $\bar{\mathbf{u}}_D = \phi \langle \bar{\mathbf{u}} \rangle^i$ and $\langle \bar{\mathbf{u}} \rangle^i$ identifies the intrinsic (liquid) average of the time-averaged velocity vector $\bar{\mathbf{u}}$.

Momentum:

$$\rho\left[\frac{\partial \bar{\mathbf{u}}_D}{\partial t} + \nabla \cdot \left(\frac{\bar{\mathbf{u}}_D \bar{\mathbf{u}}_D}{\phi}\right)\right] = -\nabla(\phi \langle \bar{p} \rangle^i) + \mu \nabla^2 \bar{\mathbf{u}}_D - \nabla \cdot (\rho \phi \langle \overline{\mathbf{u}'\mathbf{u}'} \rangle^i) - \left[\frac{\mu \phi}{K} \bar{\mathbf{u}}_D + \frac{c_F \phi \rho |\bar{\mathbf{u}}_D| \bar{\mathbf{u}}_D}{\sqrt{K}}\right] \tag{14}$$

where the last two terms in Eq. (14) represent the Darcy and Forchheimer contributions by [47]. The symbol K is the porous medium permeability, c_F is the form drag or Forchheimer coefficient, $\langle \bar{p} \rangle^i$ is the intrinsic average pressure of the fluid, and ϕ is the porosity of the porous medium.

The macroscopic Reynolds stress, $-\rho \phi \langle \overline{\mathbf{u}'\mathbf{u}'} \rangle^i$, appearing in Eq. (14) is given as

$$-\rho \phi \langle \overline{\mathbf{u}'\mathbf{u}'} \rangle^i = \mu_{t_\phi} 2 \langle \bar{D} \rangle^\nu - \frac{2}{3} \phi \rho \langle k \rangle^i \mathbf{I} \tag{15}$$

where

$$\langle \bar{D} \rangle^{v} = \tfrac{1}{2}[\nabla(\phi\langle \bar{\mathbf{u}} \rangle^{i}) + [\nabla(\phi\langle \bar{\mathbf{u}} \rangle^{i})]^{T}] \tag{16}$$

is the macroscopic deformation tensor, $\langle k \rangle^{i} = \langle \overline{\mathbf{u}'\mathbf{u}'} \rangle^{i}/2$ is the intrinsic turbulent kinetic energy, and μ_{t_ϕ}, is the turbulent viscosity, which is modeled in [27] similarly to the case of clear flow, in the form,

$$\mu_{t_\phi} = \rho c_\mu \frac{\langle k \rangle^{i^2}}{\langle \epsilon \rangle^{i}} \tag{17}$$

The intrinsic turbulent kinetic energy per unit mass and its dissipation rate are governed by the following equations:

$$\rho\left[\frac{\partial}{\partial t}(\phi\langle k \rangle^{i}) + \nabla \cdot (\bar{\mathbf{u}}_D \langle k \rangle^{i})\right] = \nabla \cdot \left[\left(\mu + \frac{\mu_{t_\phi}}{\sigma_k}\right)\nabla(\phi\langle k \rangle^{i})\right] - \rho\langle \overline{\mathbf{u}'\mathbf{u}'} \rangle^{i} : \nabla \bar{\mathbf{u}}_D + c_k \rho \frac{\phi\langle k \rangle^{i} |\bar{\mathbf{u}}_D|}{\sqrt{K}} - \rho\phi\langle \epsilon \rangle^{i} \tag{18}$$

$$\rho\left[\frac{\partial}{\partial t}(\phi\langle \epsilon \rangle^{i}) + \nabla \cdot (\bar{\mathbf{u}}_D \langle \epsilon \rangle^{i})\right] = \nabla \cdot \left[\left(\mu + \frac{\mu_{t_\phi}}{\sigma_\epsilon}\right)\nabla(\phi\langle \epsilon \rangle^{i})\right] + c_1(-\rho\langle \overline{\mathbf{u}'\mathbf{u}'} \rangle^{i} : \nabla \bar{\mathbf{u}}_D)\frac{\langle \epsilon \rangle^{i}}{\langle k \rangle^{i}} + c_2 c_k \rho \frac{\phi\langle \epsilon \rangle^{i} |\bar{\mathbf{u}}_D|}{\sqrt{K}} - c_2 \rho \phi \frac{\langle \epsilon \rangle^{i^2}}{\langle k \rangle^{i}} \tag{19}$$

where, c_k, c_1, c_2, and c_μ are nondimensional constants. The second terms on the left-hand side of Eqs. (18) and (19) represent the generation rate of $\langle k \rangle^{i}$ and $\langle \epsilon \rangle^{i}$, respectively, due to the mean gradient of $\bar{\mathbf{u}}_D$. The third terms in the same equations are the generation rates due to the action of the porous matrix (see [16]).

Similarly, macroscopic energy equations are obtained for both fluid and solid phases by applying time and volume average operators to Eqs. (3) and (4). As in the flow case, volume integration is performed over a REV, resulting in

$$(\rho c_p)_f\left[\frac{\partial \phi\langle \overline{T}_f \rangle^{i}}{\partial t} + \nabla \cdot \{\phi(\langle \bar{\mathbf{u}} \rangle^{i}\langle \overline{T}_f \rangle^{i} + \langle {}^{i}\mathbf{u}^{i}\overline{T}_f \rangle^{i} + \overline{\langle \mathbf{u}' \rangle^{i}\langle T_f' \rangle^{i}} + \langle \overline{{}^{i}\mathbf{u}'^{i}T'_f} \rangle^{i})\}\right] = \nabla \cdot \left[k_f \nabla(\phi\langle \overline{T}_f \rangle^{i}) + \frac{1}{\Delta V}\int_{A_i} \mathbf{n}_i k_f \overline{T}_f \, dA\right] + h_i a_i(\langle \overline{T}_s \rangle^{i} - \langle \overline{T}_f \rangle^{i}) \tag{20}$$

$$(\rho c_p)^{s}\left\{\frac{\partial(1-\phi)\langle \overline{T}_s \rangle^{i}}{\partial t}\right\} = \nabla \cdot \left\{k_s \nabla[(1-\phi)\langle \overline{T}_s \rangle^{i}] - \frac{1}{\Delta V}\int_{A_i} \mathbf{n}_i k_s \overline{T}_s \, dA\right\} - h_i a_i(\langle \overline{T}_s \rangle^{i} - \langle \overline{T}_f \rangle^{i}) \tag{21}$$

where, h_i and a_i are the interfacial convective heat transfer coefficient and surface area per unit volume, respectively.

2.4 Macroscopic Two-Energy Equation Modeling. In order to apply Eqs. (20) and (21) to obtain the temperature field for turbulent flow in porous media, the underscored terms have to be modeled in some way as a function of the intrinsically averaged temperature of solid phase and fluid, $\langle \overline{T}_s \rangle^{i}$ and $\langle \overline{T}_f \rangle^{i}$. To accomplish this, a gradient-type diffusion model is used for all the terms, i.e., thermal dispersion due to spatial deviations, turbulent heat flux due to temporal fluctuations, turbulent thermal dispersion due to temporal fluctuations, and spatial deviations and local conduction.

Using these gradient type diffusion models, we can write:

Turbulent heat flux:

$$-(\rho c_p)_f(\phi\overline{\langle \mathbf{u}' \rangle^{i}\langle T_f' \rangle^{i}}) = \mathbf{K}_t \cdot \nabla\langle \overline{T}_f \rangle^{i} \tag{22}$$

Thermal dispersion:

$$-(\rho c_p)_f(\phi\langle {}^{i}\bar{\mathbf{u}}^{i}\overline{T}_f \rangle^{i}) = \mathbf{K}_{\text{disp}} \cdot \nabla\langle \overline{T}_f \rangle^{i} \tag{23}$$

Turbulent thermal dispersion:

$$-(\rho c_p)_f(\phi\langle \overline{{}^{i}\mathbf{u}'^{i}T'_f} \rangle^{i}) = \mathbf{K}_{\text{disp},t} \cdot \nabla\langle \overline{T}_f \rangle^{i} \tag{24}$$

Local conduction:

$$\nabla \cdot \left[\frac{1}{\Delta V}\int_{A_i} \mathbf{n}_i k_f \overline{T}_f \, dA\right] = \mathbf{K}_{f,s} \cdot \nabla\langle \overline{T}_s \rangle^{i}$$

$$\nabla \cdot \left[\frac{1}{\Delta V}\int_{A_i} \mathbf{n}_i k_f \overline{T}_s \, dA\right] = \mathbf{K}_{s,f} \cdot \nabla\langle \overline{T}_f \rangle^{i} \tag{25}$$

For the above shown expressions, Eqs. (20) and (21) can be written as:

$$\{(\rho c_p)_f \phi\}\frac{\partial\langle \overline{T} \rangle^{i}}{\partial t} + (\rho c_p)_f \nabla \cdot (\mathbf{u}_D\langle \overline{T}_f \rangle^{i}) = \nabla \cdot \{\mathbf{K}_{\text{eff},f} \cdot \nabla\langle \overline{T}_f \rangle^{i}\} + h_i a_i(\langle \overline{T}_s \rangle^{i} - \langle \overline{T}_f \rangle^{i}) \tag{26}$$

$$\{(1-\phi)(\rho c_p)_s\}\frac{\partial\langle \overline{T} \rangle^{i}}{\partial t} = \nabla \cdot \{\mathbf{K}_{\text{eff},s} \cdot \nabla\langle \overline{T}_s \rangle^{i}\} + h_i a_i(\langle \overline{T}_s \rangle^{i} - \langle \overline{T}_f \rangle^{i}) \tag{27}$$

where, $\mathbf{K}_{\text{eff},f}$ and $\mathbf{K}_{\text{eff},s}$ are the effective conductivity tensor for fluid and solid, respectively, given by:

$$\mathbf{K}_{\text{eff},f} = \lfloor \phi k_f \rfloor \mathbf{I} + \mathbf{K}_{f,s} + \mathbf{K}_t + \mathbf{K}_{\text{disp}} + \mathbf{K}_{\text{disp},t} \tag{28}$$

$$\mathbf{K}_{\text{eff},s} = [(1-\phi)k_s]\mathbf{I} + \mathbf{K}_{s,f} \tag{29}$$

and $\mathbf{I}$ is the unit tensor. Details of interfacial convective heat transfer coefficient are presented next section.

In order to be able to apply Eq. (26), it is necessary to determine the dispersion and conductivity tensors in Eq. (28), i.e., $\mathbf{K}_{f,s}$, $\mathbf{K}_t$, $\mathbf{K}_{\text{disp}}$, and $\mathbf{K}_{\text{disp},t}$. Following Kuwahara and Nakayama [38] and Quintard et al. [5], this can be accomplished for the thermal dispersion and conductivity tensors, $\mathbf{K}_{f,s}$ and $\mathbf{K}_{\text{disp}}$, by making use of a unit cell subjected to periodic boundary conditions for the flow and a linear temperature gradient, to represent the porous medium. The dispersion and conductivity tensors are then obtained directly from the microscopic results for the unit cell, using Eqs. (23) and (25). Besides, it can be used for the following correlations for the transverse and longitudinal components of the thermal dispersion tensor, which are valid for $\text{Pe}_D \geqslant 10$:

$$\frac{(k_{\text{dis}})_{xx}}{k_f} = 2.1\frac{\text{Pe}_D}{(1-\phi)^{0.1}}, \text{ for longitudinal dispersion} \tag{30}$$

$$\frac{(k_{\text{dis}})_{yy}}{k_f} = 0.052(1-\phi)^{0.5}\,\text{Pe}_D, \text{ for transverse dispersion} \tag{31}$$

The turbulent heat flux and turbulent thermal dispersion terms, $\mathbf{K}_t$ and $\mathbf{K}_{\text{disp},t}$, which can not be determined from such a microscopic calculation, are modeled through the eddy diffusivity concept, similarly to Nakayama and Kuwahara [42]. It should be noticed that these terms arise only if the flow in the porous medium is turbulent, whereas the thermal dispersion terms exist for

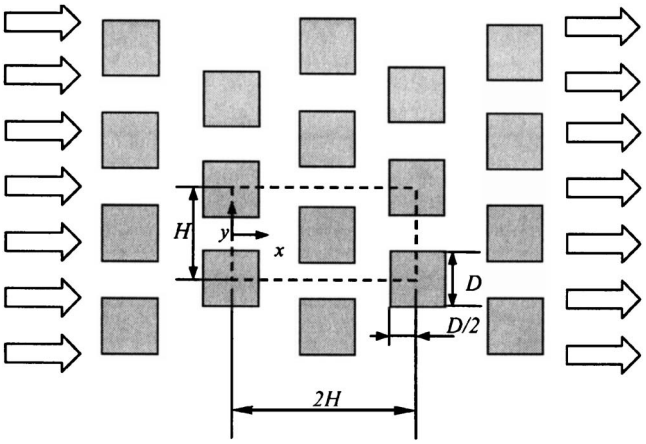

Fig. 1 Physical model and coordinate system

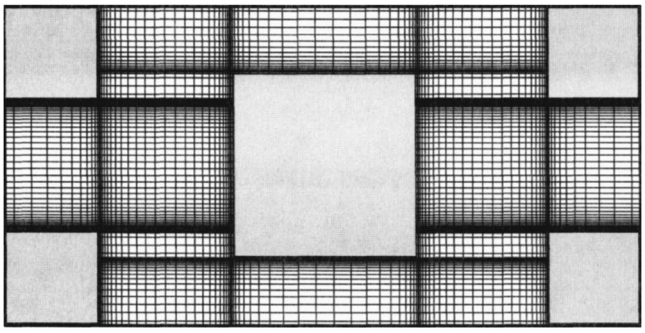

Fig. 2 Nonuniform computational grid

both laminar and turbulent flow regimes. Starting out from the time averaged energy equation coupled with the microscopic modeling for the "turbulent thermal stress tensor" through the microscopic eddy diffusivity, $\Gamma_T = \mu_t/\sigma_T$, one can write:

$$-(\rho c_p)_f \overline{\mathbf{u}' T_f'} = (\rho c_p)_f \frac{\nu_t}{\sigma_T} \nabla \bar{T}_f \tag{32}$$

where σ_T is the turbulent Prandtl number which is taken here as a constant.

Applying the volume average to the resulting equation, one obtains the macroscopic version of the "turbulent thermal stress tensor," given by:

$$-(\rho c_p)_f \langle \overline{\mathbf{u}' T_f'} \rangle^i = (\rho c_p)_f \frac{\nu_{t_\phi}}{\sigma_T} \nabla \langle \bar{T}_f \rangle^i \tag{33}$$

where we have adopted the symbol ν_{t_ϕ} to express the macroscopic version of the eddy viscosity, $\mu_{t_\phi} = \rho_f \nu_{t_\phi}$.

Equation (33) is the sum of the turbulent heat flux and the turbulent thermal dispersion found by Rocamora and de Lemos [20]. In view of the arguments given above, the turbulent heat flux and turbulent thermal dispersion components of the conductivity tensor, $\mathbf{K}_t$ and $\mathbf{K}_{\text{disp},t}$, respectively, will be expressed as:

$$\mathbf{K}_t + \mathbf{K}_{\text{disp},t} = \phi (\rho c_p)_f \frac{\nu_{t_\phi}}{\sigma_T} \mathbf{I} \tag{34}$$

2.5 Interfacial Heat Transfer Coefficient. In Eqs. (20) and (21) the heat transferred between the two phases can be modeled by means of a film coefficient h_i such that,

$$h_i a_i (\langle \overline{T_s} \rangle^i - \langle \overline{T_f} \rangle^i) = \frac{1}{\Delta V} \int_{\Lambda_i} \mathbf{n}_i \cdot k_f \nabla \overline{T_f} \, dA = \frac{1}{\Delta V} \int_{\Lambda_i} \mathbf{n}_i \cdot k_s \nabla \overline{T_s} \, dA \tag{35}$$

where, $a_i = A_i/\Delta V$.

Wakao et al. [48] obtained a heuristic correlation for closely packed bed, of particle diameter D and compared their with experimental data. This correlation for the interfacial heat transfer coefficient is given by,

$$\frac{h_i D}{k_f} = 2 + 1.1 \, \mathrm{Re}_D^{0.6} \, \mathrm{Pr}^{1/3} \tag{36}$$

For numerically determining h_i, Kuwahara et al. [7] modeled a porous medium by considering an infinite number of solid square rods of size D, arranged in a regular triangular pattern (see Fig. 1). They numerically solved the governing equations in the void region, exploiting to advantage the fact that for an infinite and geometrically ordered medium a repetitive cell can be identified. Periodic boundary conditions were then applied for obtaining the temperature distribution under fully developed flow conditions. A numerical correlation for the interfacial convective heat transfer coefficient was proposed by Kuwahara et al. [7] for laminar flow as,

$$\frac{h_i D}{k_f} = \left(1 + \frac{4(1-\phi)}{\phi}\right) + \frac{1}{2}(1-\phi)^{1/2} \, \mathrm{Re}_D^{0.6} \, \mathrm{Pr}^{1/3}, \text{ valid for } 0.2 < \phi < 0.9 \tag{37}$$

Equation (37) is based on porosity dependency and is valid for packed beds of particle diameter D.

Saito and de Lemos [13] obtained the interfacial heat transfer coefficient for laminar flows though an infinite square rod; this same physical model will be used here for obtaining the interfacial heat transfer coefficient h_i for turbulent flows.

The flow through an infinite square rod can be associated with flow across a bundle of tubes. Furthermore the heat transfer coefficient related to a tube is determined by its position in the package. The tube rows of a bundle are either aligned or staggered in the direction of the fluid velocity. In this work the geometric arrangement is staggered (see Fig. 1). For the staggered configuration Zhukauskas [27] has proposed a correlation of the form,

$$\frac{h_i D}{k_f} = 0.022 \, \mathrm{Re}_D^{0.84} \, \mathrm{Pr}^{0.36} \tag{38}$$

where the values 0.022 and 0.84 are constants for tube bank in cross flow and for this particular case $2 \times 10^5 < \mathrm{Re}_D < 2 \times 10^6$.

3 Periodic Cell and Boundary Conditions

The macroscopic hydrodynamic and thermodynamic behavior of practical interest can be obtained from the direct application of the first principles to viscous flow and heat transfer at a pore scale. In reality, however, it is impossible to resolve the details of the flow and heat transfer fields within a real porous medium. Nakayama et al. [8] and Kuwahara et al. [7] modeled a porous medium in terms of obstacles arranged in a regular pattern, and solved the set of the microscopic governing equations, exploiting periodic boundary conditions.

In order to evaluate the numerical tool to be used in the determination of the film coefficient given by Eq. (35), a test case was run for obtaining the flow field in a periodic cell, which is here assumed to represent the porous medium. Consider a macroscopically uniform flow through an infinite number of square rods of lateral size D, placed in a staggered arrangement and maintained at constant temperature T_w. The periodic cell or representative elementary volume, ΔV is schematically showed in Fig. 1 and has dimensions $2H \times H$. Computations within this cell were carried out using a nonuniform grid, as shown in Fig. 2, to ensure that the

results were grid independent. The Reynolds number $\mathrm{Re}_D = \rho \bar{\mathbf{u}}_D D/\mu$ was varied from 10^4 to 10^7 and the porosity, $\phi = 1 - (D/H)^2$.

The numerical method utilized to discretize the flow and energy equations in the unit cell is the finite control volume approach. The SIMPLE method of Patankar [49] was used for handling Eqs. (1)–(4) the velocity-pressure coupling. Convergence was monitored in terms of the normalized residue for each variable. The maximum residue allowed for convergence check was set to 10^{-9}, being the variables normalized by appropriate reference values.

For fully developed flow in the cell of Fig. 1, the velocity at exit ($x/H=2$) must be identical to that at the inlet ($x/H=0$). Temperature profiles, however, are only identical at both the cell exit and inlet if presented in terms of an appropriate nondimensional variable. The situation is analogous to the case of forced convection in a channel with isothermal walls. Due to the periodicity of the model and a single structural unit as indicated in Fig. 1 may be taken as a calculation domain. The equations used for turbulent flow in the unit cell are Eqs. (5), (6), and (11).

Thus, boundary conditions and periodic constraints are given by:

On the solid walls (Low Re Model):

$$\bar{u} = 0, \quad k = 0, \quad \epsilon = \nu \frac{\partial^2 k}{\partial y^2}, \quad \bar{T} = \bar{T}_w \tag{39}$$

On the solid walls (High Re Model):

$$\frac{\bar{u}}{u_\tau} = \frac{1}{\kappa} \ln(y^+ E), \quad k = \frac{u_\tau^2}{c_\mu^{1/2}}, \quad \epsilon = \frac{c_\mu^{3/4} k_w^{3/2}}{\kappa y_w},$$

$$q_w = \frac{(\rho c_p)_f c_\mu^{1/4} k_w^{1/2} (\bar{T} - \bar{T}_w)}{\left(\frac{\mathrm{Pr}_t}{\kappa} \ln(y_w^+) + c_Q(\mathrm{Pr}) \right)} \tag{40}$$

where,

$$u_\tau = \left(\frac{\tau_w}{\rho} \right)^{1/2}, \quad y_w^+ = \frac{y_w u_\tau}{\nu},$$

$$c_Q = 12.5\,\mathrm{Pr}^{2/3} + 2.12 \ln(\mathrm{Pr}) - 5.3 \text{ for } \mathrm{Pr} > 0.5$$

where, Pr and Pr_t are Prandtl and turbulent Prandtl number, respectively, q_w is wall heat flux, u_τ is wall-friction velocity, y_w is the coordinate normal to wall, κ is a constant for turbulent flow past smooth impermeable walls or von Kármán's constant, and E is an integration constant that depends on the roughness of the wall. For smooth walls with constant shear stress $E=9$.

On the symmetry planes:

$$\frac{\partial \bar{u}}{\partial y} = \frac{\partial \bar{v}}{\partial y} = \frac{\partial k}{\partial y} = \frac{\partial \epsilon}{\partial y} = 0 \tag{41}$$

where $\bar{u}$ and $\bar{v}$ are components of $\mathbf{u}$.

On the periodic boundaries:

$$\bar{u}|_{\mathrm{inlet}} = \bar{u}|_{\mathrm{outlet}}, \quad \bar{v}|_{\mathrm{inlet}} = \bar{v}|_{\mathrm{outlet}}, \quad k|_{\mathrm{inlet}} = k|_{\mathrm{outlet}}, \quad \epsilon|_{\mathrm{inlet}} = \epsilon|_{\mathrm{outlet}} \tag{42}$$

$$\theta|_{\mathrm{inlet}} = \theta|_{\mathrm{outlet}} \Leftrightarrow \left. \frac{\bar{T} - \bar{T}_w}{\bar{T}_B(x) - \bar{T}_w} \right|_{\mathrm{inlet}} = \left. \frac{\bar{T} - \bar{T}_w}{\bar{T}_B(x) - \bar{T}_w} \right|_{\mathrm{outlet}} \tag{43}$$

The bulk mean temperature of the fluid is given by:

$$\bar{T}_B(x) = \frac{\int \bar{u} \bar{T}\, dy}{\int \bar{u}\, dy} \tag{44}$$

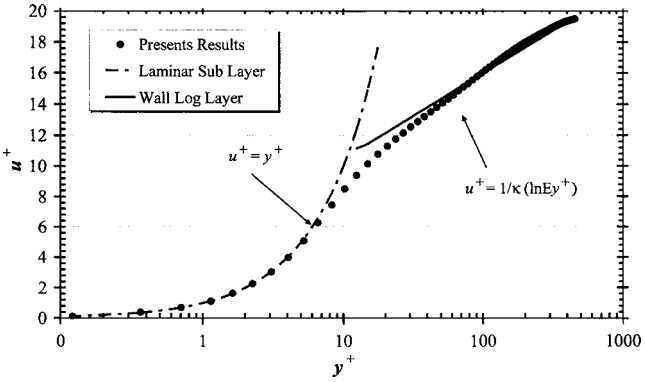

Fig. 3 Velocity profile in fully developed pipe flow

Computations are based on the Darcy velocity, the length of structural unit H, and the temperature difference $(\bar{T}_B(x) - \bar{T}_w)$, as references scales.

3.1 Film Coefficient h_i. Determination of h_i is here obtained by calculating, for the unit cell of Fig. 1, an expression given as,

$$h_i = \frac{Q_{\mathrm{total}}}{A_i \Delta T_{\mathrm{ml}}} \tag{45}$$

where $A_i = 8Dx1$. The overall heat transferred in the cell, Q_{total}, is giving by,

$$Q_{\mathrm{total}} = (H - D) \rho \bar{u}_B c_p (\bar{T}_B|_{\mathrm{outlet}} - \bar{T}_B|_{\mathrm{inlet}}) \tag{46}$$

The bulk mean velocity of the fluid is given by:

$$\bar{u}_B(x) \frac{\int \bar{u}\, dy}{\int dy} \tag{47}$$

and the logarithm mean temperature difference, ΔT_{ml} is,

$$\Delta T_{\mathrm{ml}} = \frac{(\bar{T}_w - \bar{T}_B|_{\mathrm{outlet}}) - (\bar{T}_w - \bar{T}_B|_{\mathrm{inlet}})}{\ln[(\bar{T}_w - \bar{T}_B|_{\mathrm{outlet}})(\bar{w} - \bar{T}_B|_{\mathrm{inlet}})]} \tag{48}$$

Equation (46) represents an overall heat balance on the entire cell and associates the heat transferred to the fluid to a suitable temperature difference ΔT_{ml}. As mentioned earlier, Eqs. (1)–(4) were numerically solved in the unit cell until conditions (42) and (43) were satisfied.

4 Results and Discussion

4.1 Periodic Flow. Results for velocity and temperature fields were obtained for different Reynolds numbers. In order to assure that the flow was hydrodynamically and thermally developed in the periodic cell of Fig. 1, the governing equations were solved repetitively in the cell, taking the outlet profiles for $\bar{\mathbf{u}}$ and θ at the exit and plugging them back at the inlet. In the first run, uniform velocity and temperature profiles were set at the cell entrance for $\mathrm{Pr}=1$ giving $\theta=1$ at $x/H=0$. Then, after convergence of the flow and temperature fields, $\bar{\mathbf{u}}$ and θ at $x/H=2$ were used as inlet profiles for a second run, corresponding to solving again the flow for a similar cell beginning in $x/H=2$. Similarly, a third run was carried out and again outlet results, this time corresponding to an axial position $x/H=4$, were recorded. This procedure was repeated several times until $\bar{\mathbf{u}}$ and θ did not differ substantially at both inlet and outlet positions. Figure 3 further shows that the velocity profile here obtained in with a low Re model has a good

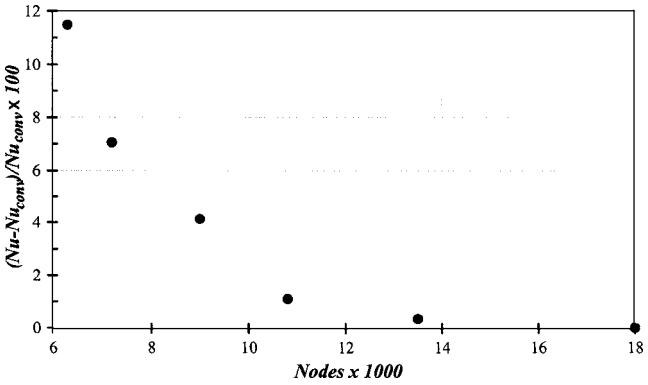

Fig. 4 Grid independence study

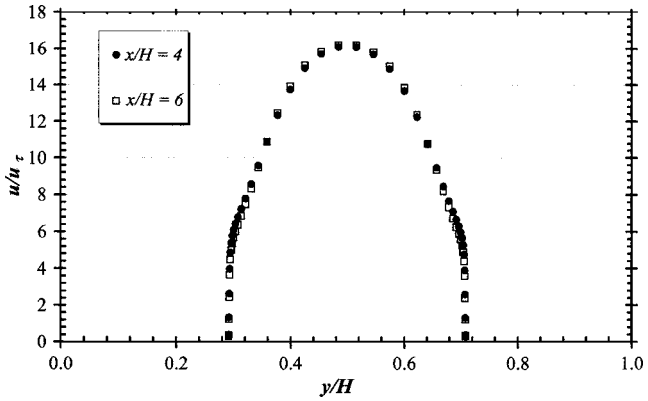

Fig. 5 Dimensionless velocity profile for Pr=1 and $Re_D=5\times10^4$

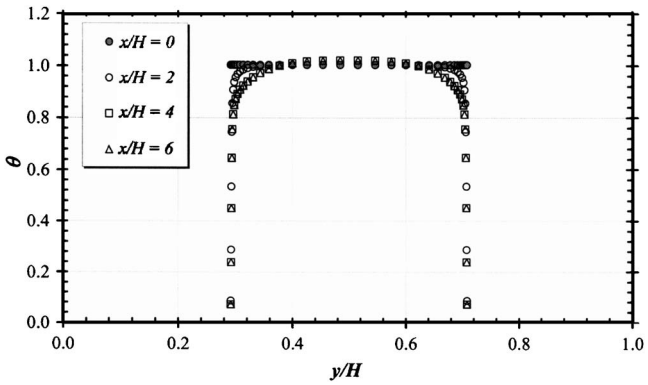

Fig. 6 Dimensionless temperature profile for Pr=1 and $Re_D=5\times10^4$

agreement within the laminar and the wall log layers.

Grid independence studies are summarized in Fig. 4, which presents results for Nu as a function of the number of grid points. The subscript conv refers to the asymptotic value as the grid increases. The figure indicates that for grids greater than 12,000, errors in Nu are less that 1%. For that, all results presented below considered this grid size.

Nondimensional velocity and temperature profiles are shown in Figs. 5 and 6, respectively, showing that the periodicity constraints imposed by Eqs. (42) and (43) was satisfied for $x/H>4$. For the entrance region ($0<x/H<4$), θ profiles change with length x/H being essentially invariable after this distance. Under this condition of constant θ profile, the flow was considered to be macroscopically developed for Re_D up to 10^7.

For the low Re model, the first node adjacent to the wall requires that the nondimensional wall distance be such that $y^+=u_\tau y\rho/\mu\leqslant1$. To accomplish this requirement, the grid needs a greater number of points close to the wall leading to computational meshes of large sizes. As a further code validation for turbulent flow calculation, which uses the $k-\epsilon$ model, a developing turbulent channel flow has been solved for $Re=5\times10^4$, where Re is based on the duct hydraulic diameter.

4.2 Developed Flow and Temperature Fields. Macroscopically developed flow field for Pr=1 and $Re_D=5\times10^4$ is presented in Fig. 5, corresponding to $x/D=6$ at the cell inlet. The expression "macroscopically developed" is used herein to account for the fact that periodic flow has been achieved at that axial position. Figures 7–9 show distributions of pressure, isotherms, and turbulence kinetic energy in a microscopic porous structure, obtained at $Re_D=10^5$ for cases of $\phi=0.65$. Pressure increases at the front face of the square rod and drastically decreases around the corner, as can be seen from the pressure contours shown in Fig. 7.

Temperature distribution is shown in Fig. 8. Colder fluid impinges on the left-hand side of the rod yielding strong temperature gradients on that face. Downstream the obstacles, fluid recirculation smooths temperature gradients and deforms isotherms within the mixing region. When the Reynolds number is sufficiently high (not shown here), thermal boundary layers cover the rod surfaces indicating that convective heat transfer overwhelms thermal diffusion. Figure 9 presents levels of turbulence kinetic energy, which are higher around the rod corners where a strong shear layer is formed. Further downstream the rods in the weak region, steep velocity gradients appear due to flow deceleration, also increasing the local level of k.

Once fully developed flow and temperature fields are achieved, for the fully developed condition ($x>6H$), bulk temperatures were calculated according to Eq. (44), at both inlet and outlet positions. They were then used to calculate h_i using Eqs. (45)–(48). Results for h_i are plotted in Fig. 10 for Re_D up to 10^7. Also plotted in this figure are results computed with correlation (37) by Kuwahara et al. [7] using $\phi=0.65$. The figure seems to

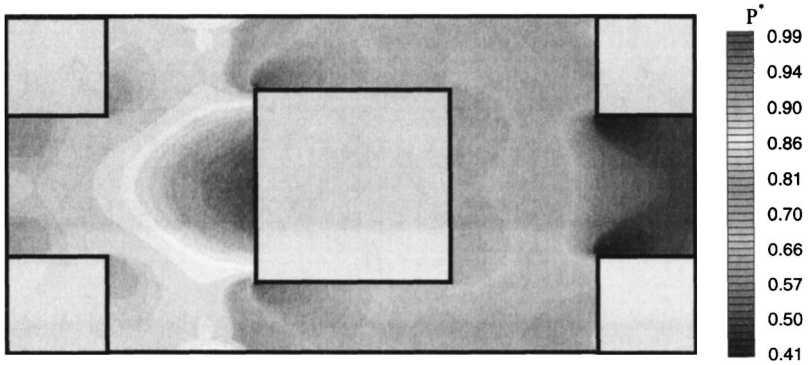

Fig. 7 Nondimensional pressure field for $Re_D=10^5$ and $\phi=0.65$

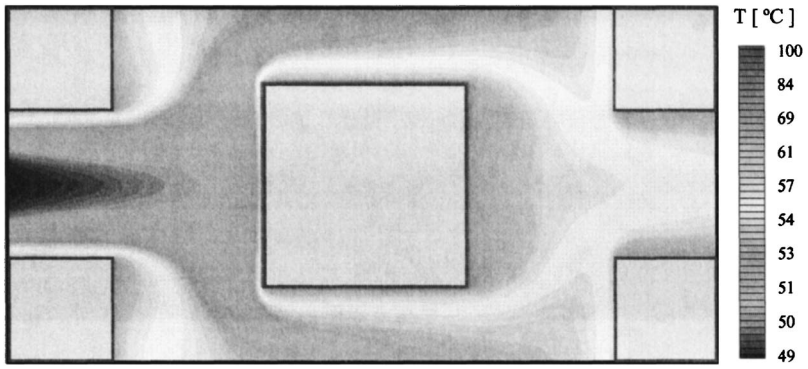

Fig. 8 Isotherms for Pr=1, $Re_D=10^5$, and $\phi=0.65$

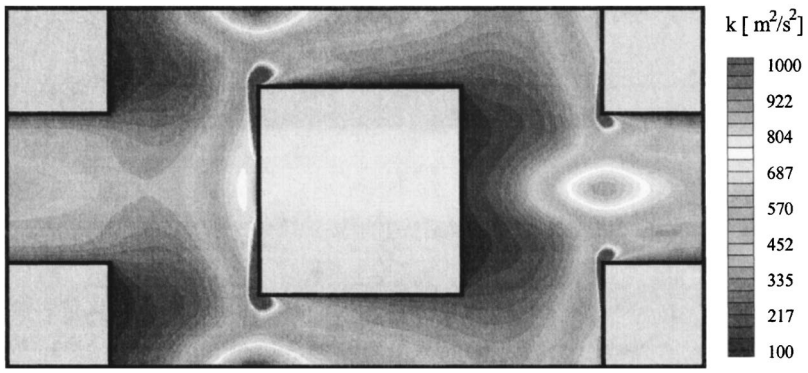

Fig. 9 Turbulence kinetic energy for $Re_D=10^5$ and $\phi=0.65$

indicate that both computations show a reasonable agreement for laminar results. In addition, numerical results for turbulent flow using low and High Re models are also presented in this figure.

Figure 11 shows numerical results for the interfacial convective heat transfer coefficient for various porosities ($\phi=0.44$, $\phi=0.65$, and $\phi=0.90$). Results for h_i are plotted for Re_D up to 10^7. In order to obtain a correlation for h_i in the turbulent regime, all curves were first collapsed after plotting them in terms of Re_D/ϕ, as shown in Fig. 12. Furthermore, the least squares technique was applied in order to determine the best correlation, which lead to a minimum overall error. Thus, the following expression is here proposed:

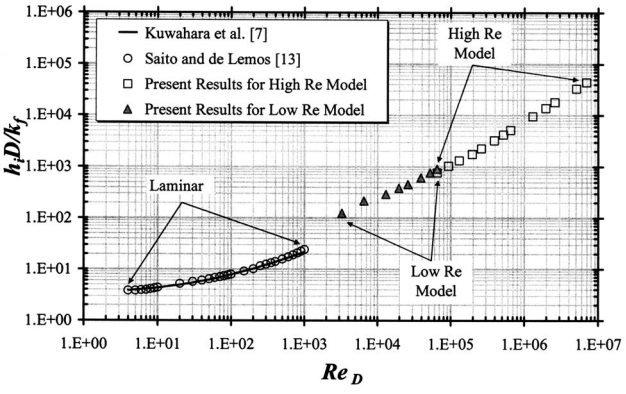

Fig. 10 Effect of Re_D on h_i for Pr=1 and $\phi=0.65$

$$\frac{h_i D}{k_f} = 0.08\left(\frac{Re_D}{\phi}\right)^{0.8} Pr^{1/3} \quad \text{for}$$

$$1.0\times 10^4 < \frac{Re_D}{\phi} < 2.0\times 10^7 \quad \text{valid for}$$

$$0.2 < \phi < 0.9 \tag{49}$$

Equation (49), which gives the heat transfer coefficient for turbulent flow, is compared with numerical results obtained with low and high Re models. Such comparison is presented in Fig. 13, which also shows computations using correlations given by Eqs. (36) and (37) by Wakao et al. [48] and Zhukauskas [50], respectively. The agreement between the present correlation, other correlations in the literature, and the numerical simulations stimulates further investigation on this subject, contributing towards the building of a more general expression for the interfacial heat transfer coefficient for porous media.

5 Concluding Remarks

A computational procedure for determining the convective coefficient of heat exchange between the porous substrate and the working fluid for a porous medium was detailed. As a preliminary result, macroscopically uniform laminar and turbulent flow through a periodic cell of isothermal square rods was computed, considering periodical velocity and temperature fields. Quantitative agreement was obtained when comparing laminar results herein with simulations by Kuwahara et al. [7]. For turbulent flows, low and high Reynolds turbulence models were employed in order to obtain the interfacial heat transfer coefficient. A correlation was then proposed for such coefficients. Further work will be carried out in order to simulate fully turbulent flow and heat transfer in a porous medium formed by arrays of elliptic, cylin-

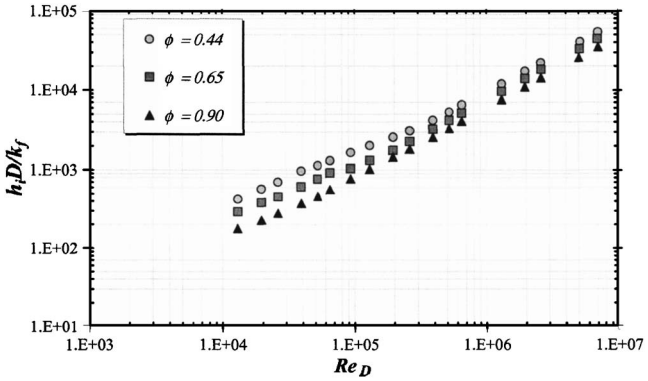

Fig. 11 Effect of porosity on h_i for Pr=1

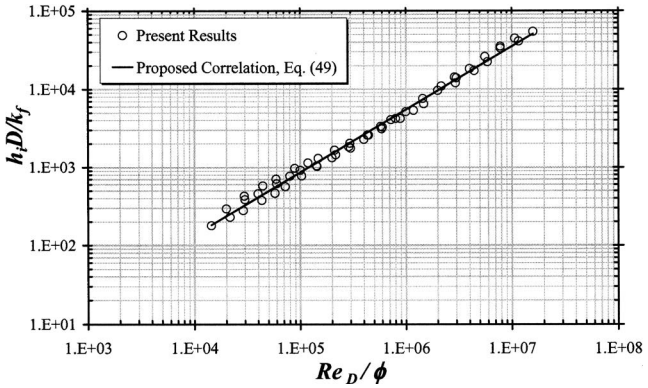

Fig. 12 Comparison of the numerical results and proposed correlation

drical and transverse elliptic rods, displaced in in-line as well as staggered arrangements. Ultimately, it is expected that a more general correlation for h_i be obtained to be used in conjunction with macroscopic two-energy equation models.

Nomenclature

A_i = interface total area between the fluid and solid
c_F = Forchheimer coefficient
c_p = fluid specific heat
D = square rods of lateral size
h_i = interfacial convective heat transfer coefficient
H = periodic cell height
$\mathbf{I}$ = unit tensor
K = permeability
k = turbulence kinetic energy per unit mass
k_f = fluid thermal conductivity
k_s = solid thermal conductivity
$\mathbf{K}_{\text{disp}}$ = dispersion conductivity tensor
$\mathbf{K}_{f,s}$ = two-equation model effective thermal conductivity tensor in fluid phase
$\mathbf{K}_{s,f}$ = two-equation model effective thermal conductivity tensor in solid phase
$\mathbf{K}_t$ = turbulence conductivity tensor
$\mathbf{K}_{\text{disp},t}$ = turbulent dispersion tensor
Nu = Interfacial Nusselt number; $\text{Nu}=h_i D/k_f$
P = pressure
P^* = $P^*(P-P_{\min})/(P_{\max}-P_{\min})$, nondimensional Pressure
Pr = $\text{Pr}=\nu/\alpha$, Prandtl number
Pe_D = Peclet number based on D and the macroscopically uniform velocity

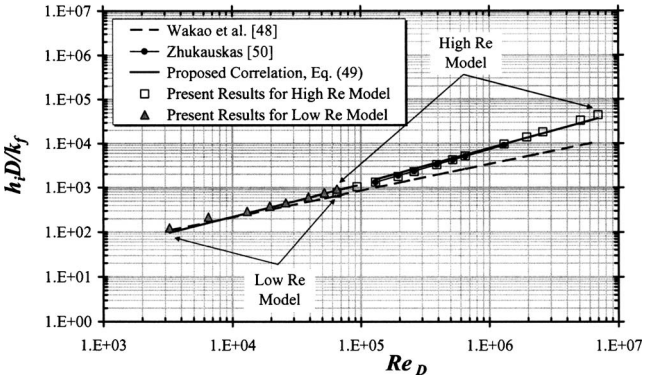

Fig. 13 Comparison of the numerical results and various correlations for ϕ=0.65

Re_D = Reynolds number based on D and the macroscopically uniform velocity
T = temperature
$\bar{T}$ = time averaged temperature
$\mathbf{u}$ = microscopic velocity
$\mathbf{u}_D$ = Darcy or superficial velocity (volume average of $\mathbf{u}$)

Greek Symbols

α = fluid thermal diffusivity
ΔV = representative elementary volume
ΔV_f = fluid volume inside ΔV
μ = fluid dynamic viscosity
μ_t = eddy viscosity
μ_{t_ϕ} = macroscopic eddy viscosity
ν = fluid kinematic viscosity
ρ = fluid density
θ = dimensionless temperature
ϕ = $\phi=\Delta V_f/\Delta V$, porosity
σ_T = turbulent Prandtl number
φ = general variable
$\langle\varphi\rangle^i$ = intrinsic average
$\langle\varphi\rangle^v$ = volume average
$^i\varphi$ = spatial deviation

Acknowledgment

The authors are thankful to CNPq and FAPESP, Brazil, for their financial support during the course of this research.

References

[1] Schumann, T. E. W., 1929, "Heat Transfer: Liquid Flowing Through a Porous Prism," J. Franklin Inst., **208**, pp. 405–416.
[2] Quintard, M., 1998, "Modeling Local Non-Equilibrium Heat Transfer in Porous Media," in *Proc. 11th Int. Heat Transfer Conf.*, Kyongyu, Korea, Vol. 1, pp. 279–285.
[3] Kuznetsov, A. V., 1998, "Thermal Nonequilibrium Forced Convection in Porous Media," Chap. 5 in *Transport Phenomena in Porous Media*, D. B. Ingham and I. Pop, eds., Elsevier, Oxford, pp. 103–129.
[4] Kaviany, M., 1995, *Principles of Heat Transfer in Porous Media*, 2nd ed., Springer, New York.
[5] Quintard, M., Kaviany, M., and Whitaker, S., 1997, "Two-Medium Treatment of Heat Transfer in Porous Media: Numerical Results for Effective Properties," Adv. Water Resour., **20**, pp. 77–94.
[6] Ochoa-Tapia, J. A., and Whitaker, S., 1997, "Heat Transfer at the Boundary Between a Porous Medium and a Homogeneous Fluid," Int. J. Heat Mass Transfer, **40**, pp. 2691–2707.
[7] Kuwahara, F., Shirota, M., and Nakayama, A., 2001, "A Numerical Study of Interfacial Convective Heat Transfer Coefficient in Two-Energy Equation Model for Convection in Porous Media," Int. J. Heat Mass Transfer, **44**, pp. 1153–1159.
[8] Nakayama, A., Kuwahara, F., Sugiyama, M., and Xu, G., 2001, "A Two-Energy Equation Model for Conduction and Convection in Porous Media," Int. J. Heat Mass Transfer, **44**, pp. 4375–4379.
[9] Hsu, C. T., 1999, "A Closure Model for Transient Heat Conduction in Porous

Media," ASME J. Heat Transfer, **121**, pp. 733–739.
[10] Nield, D. A., and Bejan, A., 1992, *Convection in Porous Media*, Springer, New York.
[11] Bear, J., 1972, *Dynamics of Fluids in Porous Media*, American Elsevier, New York.
[12] Sahraouri, M., and Kaviany, M., 1994, "Direct Simulation Versus Volume-Averaged Treatment of Adiabatic, Premixed Flame in a Porous Medium," Int. J. Heat Mass Transfer, **37**(18), pp. 2817–2834.
[13] Saito, M. B., and de Lemos, M. J. S., 2005, "Interfacial Heat Transfer Coefficient for NonEquilibrium Convective Transport in Porous Media," Int. Commun. Heat Mass Transfer, **32**(5), pp. 667–677.
[14] Gray, W. G., and Lee, P. C. Y., 1977, "On the Theorems for Local Volume Averaging of Multiphase System," Int. J. Multiphase Flow, **3**, pp. 333–340.
[15] Pedras, M. H. J., and de Lemos, M. J. S., 2000, "On the Definition of Turbulent Kinetic Energy for Flow in Porous Media," Int. Commun. Heat Mass Transfer, **27**(2), pp. 211–220.
[16] Pedras, M. H. J., and de Lemos, M. J. S., 2001, "Macroscopic Turbulence Modeling for Incompressible Flow Through Undeformable Porous Media," Int. J. Heat Mass Transfer, **44**(6), pp. 1081–1093.
[17] Pedras, M. H. J., and de Lemos, M. J. S., 2001, "Simulation of Turbulent Flow in Porous Media Using a Spatially Periodic Array and a Low-Re Two-Equation Closure," Numer. Heat Transfer, Part A, **39**(1), pp. 35–59.
[18] Pedras, M. H. J., and de Lemos, M. J. S., 2001, "On the Mathematical Description and Simulation of Turbulent Flow in a Porous Medium Formed by an Array of Elliptic Rods," J. Fluids Eng., **123**(4), pp. 941–947.
[19] Pedras, M. H. J., and de Lemos, M. J. S., 2003, "Computation of Turbulent Flow in Porous Media Using a Low Reynolds k-ϵ Model and an Infinite Array of Transversally-Displaced Elliptic Rods," Numer. Heat Transfer, Part A, **43**(6), pp. 585–602.
[20] Rocamora, F. D. Jr., and de Lemos, M. J. S., 2000, "Analysis of Convective Heat Transfer of Turbulent Flow in Saturated Porous Media," Int. Commun. Heat Mass Transfer, **27**(6), pp. 825–834.
[21] de Lemos, M. J. S., and Braga, E. J., 2003, "Modeling of Turbulent Natural Convection in Saturated Rigid Porous Media," Int. Commun. Heat Mass Transfer, **30**(5), pp. 615–624.
[22] Braga, E. J., and de Lemos, M. J. S., 2004, "Turbulent Natural Convection in a Porous Square Cavity Computed with a Macroscopic k-ϵ Model," Int. J. Heat Mass Transfer, **47**(26), pp. 5639–5650.
[23] Braga, E. J., and de Lemos, M. J. S., 2005, "Heat Transfer in Enclosures Having a Fixed Amount of Solid Material Simulated with Heterogeneous and Homogeneous Models," Int. J. Heat Mass Transfer, **48**(23-24), pp. 4748–4765.
[24] Braga, E. J., and de Lemos, M. J. S., 2000, "Laminar Natural Convection in Cavities Filled with Circular and Square Rods," Int. Commun. Heat Mass Transfer, **32**(10), pp. 1289–1297.
[25] de Lemos, M. J. S., and Mesquita, M. S., 2003, "Turbulent Mass Transport in Saturated Rigid Porous Media," Int. Commun. Heat Mass Transfer, **30**(1), pp. 105–113.
[26] de Lemos, M. J. S., and Tofaneli, L. A., 2004, "Modeling of Double-Diffusive Turbulent Natural Convection in Porous Media," Int. J. Heat Mass Transfer, **47**(19-20), pp. 4221–4231.
[27] de Lemos, M. J. S., and Pedras, M. H. J., 2001, "Recent Mathematical Models for Turbulent Flow for Saturated Rigid Porous Media," J. Fluids Eng., **123**(4), pp. 935–940.
[28] Silva, R. A., and de Lemos, M. J. S., 2003, "Numerical Analysis of the Stress Jump Interface Condition for Laminar Flow over a Porous Layer," Numer. Heat Transfer, Part A, **43**(6), pp. 603–617.
[29] Silva, R. A., and de Lemos, M. J. S., 2003, "Turbulent Flow in a Channel Occupied by a Porous Layer Considering the Stress Jump at the Interface," Int. J. Heat Mass Transfer, **46**(26), pp. 5113–5121.
[30] de Lemos, M. J. S., 2005, "Turbulent Kinetic Energy Distribution Across the Interface Between a Porous Medium and a Clear Region," Int. Commun. Heat Mass Transfer, **32**(1-2), pp. 107–115.
[31] de Lemos, M. J. S., and Silva, R. A., 2006, "Turbulent Flow Over A Layer Of A Highly Permeable Medium Simulated With A Diffusion-Jump Model For The Interface," Int. J. Heat Mass Transfer, **49**(3-4), pp. 546–556.
[32] de Lemos, M. J. S., and Rocamora, F. D., 2002, "Turbulent Transport Modeling for Heated Flow in Rigid Porous Media, in *Proceedings of the Twelfth International Heat Transfer Conference*, Grenoble, France, August 18–23, pp. 791–795.
[33] Launder, B. E., and Spalding, D. B., 1974, "The Numerical Computation of Turbulent Flows," Comput. Methods Appl. Mech. Eng., **3**, pp. 269–289.
[34] Hsu, C. T., and Cheng, P., 1990, "Thermal Dispersion in a Porous Medium," Int. J. Heat Mass Transfer, **33**, pp. 1587–1597.
[35] Whitaker, S., 1966, "Equations of Motion in Porous Media," Chem. Eng. Sci., **21**, pp. 291–300.
[36] Whitaker, S., 1967, "Diffusion and Dispersion in Porous Media," AIChE J., **13**(3), pp. 420–427.
[37] Masuoka, T., and Takatsu, Y., 1996, "Turbulence Model for Flow Through Porous Media," Int. J. Heat Mass Transfer, **39**(13), pp. 2803–2809.
[38] Kuwahara, F., Nakayama, A., and Koyama, H., 1996, "A Numerical Study of Thermal Dispersion in Porous Media," ASME J. Heat Transfer, **118**, pp. 756–761.
[39] Kuwahara, F., and Nakayama, A., 1998, "Numerical Modeling of Non-Darcy Convective Flow in a Porous Medium, *Heat Transfer 1998, Proceedings of the 11th Int. Heat Transf. Conf.*, Kyongyu, Korea, Taylor and Francis, Washington, D.C., Vol. 4, pp. 411–416.
[40] Kuwahara, F., Kameyama, Y. Yamashita, S. and Nakayama, A., 1998, "Numerical Modeling of Turbulent Flow in Porous Media Using a Spatially Periodic Array," J. Porous Media, **1**(1), pp. 47–55.
[41] Ergun, S., 1952, "Fluid Flow Through Packed Columns," Chem. Eng. Prog., **48**, pp. 89–94.
[42] Nakayama, A., and Kuwahara, F., 1999, "A Macroscopic Turbulence Model for Flow in a Porous Medium," J. Fluids Eng., **121**, pp. 427–433.
[43] Lee, K., and Howell, J. R., 1987, "Forced Convective and Radiative Transfer Within a Highly Porous Layer Exposed to a Turbulent External Flow Field," in *Proceedings of the 1987 ASME-JSME Thermal Engineering Joint Conf.*, Honolulu, Hawaii, ASME, New York, Vol. 2, pp. 377–386.
[44] Antohe, B. V., and Lage, J. L., 1997, "A General Two-Equation Macroscopic Turbulence Model for Incompressible Flow in Porous Media," Int. J. Heat Mass Transfer, **40**(13), pp. 3013–3024.
[45] Getachewa, D., Minkowycz, W. J., and Lage, J. L., 2000, "A Modified Form of the k-ϵ Model for Turbulent Flow of a Incompressible Fluid in Porous Media," Int. J. Heat Mass Transfer, **43**, pp. 2909–2915.
[46] Slattery, J. C., 1967, "Flow of Viscoelastic Fluids Through Porous Media," AIChE J., **13**, pp. 1066–1071.
[47] Forchheimer, P., 1901, "Wasserbewegung durch Boden," Z. Ver. Deutsch. Ing., **45**, pp. 1782–1788.
[48] Wakao, N., Kaguei, S., and Funazkri, T., 1979, "Effect of Fluid Dispersion Coefficients on Particle-to-Fluid Heat Transfer Coefficients in Packed Bed," Chem. Eng. Sci., **34**, pp. 325–336.
[49] Patankar, S. V., 1980, *Numerical Heat Transfer and Fluid Flow*, Hemisphere, Washington, D.C.
[50] Zhukauskas, A., 1972, "Heat Transfer from Tubes in Cross Flow," Adv. Heat Transfer, **8**, pp. 93–160.